

GraphGDel: Constructing and Learning Graph Representations of Genome-Scale Metabolic Models for Growth-Coupled Gene Deletion Prediction

Ziwei Yang¹, Takeyuki Tamura¹

¹ *Bioinformatics Center, Institute for Chemical Research, Kyoto University, Kyoto, Japan*

Abstract—In genome-scale constraint-based metabolic models, gene deletion strategies are essential for achieving growth-coupled production, where cell growth and target metabolite synthesis occur simultaneously. Despite the inherently networked nature of genome-scale metabolic models, existing computational approaches rely primarily on sequential data and lack graph representations that capture their complex relationships, as both well-defined graph constructions and learning frameworks capable of exploiting them remain largely unexplored. To address this gap, we present a twofold solution. First, we introduce a systematic pipeline for constructing graph representations from constraint-based metabolic models. Second, we develop a deep learning framework that integrates these graph representations with gene and metabolite sequence data to predict growth-coupled gene deletion strategies. Across three metabolic models of varying scale, our approach consistently outperforms established baselines, achieves improvements of 14.04%, 16.26%, and 13.18% in overall accuracy. The source code and example datasets are available at: <https://github.com/MetNetComp/GraphGDel>.

Index Terms—Biology and genetics, Machine learning, Graphs and networks, Scientific databases.

I. INTRODUCTION

Computational approaches are central to metabolic engineering, enabling the systematic design and optimization of microbial strains [1], [2], [3], [4], [5]. A key application is computational strain design, which employs mathematical models to simulate cellular metabolism and guide the optimization of target metabolite biosynthesis. Among available modeling frameworks, the **constraint-based model** is widely used in genome-scale metabolic engineering. It comprises two key components: (1) a metabolic network and (2) gene–protein–reaction (GPR) rules. The metabolic network defines the biochemical transformations among metabolites, catalyzed by enzymes encoded by specific genes. GPR rules, typically expressed as Boolean functions, describe the logical relationships between genes, proteins, and reactions, specifying whether a reaction is active based on gene presence. By altering gene content, the metabolic network can be systematically reprogrammed. One widely applied operation is **gene deletion**, which disables specific reactions by removing genes that encode essential enzymes. This approach, central to metabolic engineering, enables the rational rewiring of metabolism to enhance the biosynthesis of target compounds.

In constraint-based simulations of gene deletions, the objective is not merely to increase the production of a target metabolite, but to achieve **growth-coupled production**—a state in which the synthesis of the target metabolite is coupled with cellular growth. This coupling is critical for industrial biotech applications, as microorganism strains with higher growth rates are more likely to dominate during repeated passaging,

thereby ensuring stable and sustained metabolite production over time. However, under native metabolic conditions, only a limited number of metabolites naturally exhibit growth-coupling. To extend this property to a broader range of target compounds, it is necessary to design **gene deletion strategies** that reconfigure the metabolic network to enforce growth-coupled production [6].

To this end, a range of computational methods have been developed over the past decade to identify gene deletion strategies capable of enabling growth-coupled phenotypes [7], [8], [9], [10], [11], [12], [13], [14], [15]. These strategies have been successfully applied in real-world contexts, facilitating the development of engineered strains for applications, including biofuel production and the industrial biosynthesis of platform chemicals [16], [17], [18]. Despite these advances, calculating gene deletion strategies *de novo* remains computationally intensive, particularly for genome-scale metabolic models that encompass complex network structures and GPR associations involving numerous genes. In response, recent efforts have focused not only on developing more mathematically efficient algorithms to accelerate these computations, but also on establishing databases to store and manage strain design data, thereby enabling more scalable and effective solutions. One prominent example is *MetNetComp* database [19], the first web-based platform to curate gene deletion strategies for growth-coupled production within constraint-based metabolic models. *MetNetComp* extends the *gDel_minRN* method [15] to compute gene deletion strategies that enable growth coupling, supporting both minimal and maximal gene deletion configurations. Currently, it hosts a comprehensive repository of over 85,000 gene deletion strategies spanning a wide range of metabolites and multiple constraint-based models from diverse species. Such resources are essential not only for meeting the growing demand for gene deletion analysis but also for enabling new paradigms in strain design, including data-driven approaches to gene deletion strategy development.

Designing data-driven approaches for gene deletion strategy development remains a non-trivial task, with a central challenge being the effective extraction and utilization of information from existing gene deletion strategy databases. The first effort in this direction, *DBgDel* [20], addressed this challenge by summarizing known maximal gene deletion strategies from the database and using them as constraints to limit the search space during optimization. This method strikes a favorable balance between computational efficiency and success rate when applied to genome-scale metabolic models. However, *DBgDel* relies on hand-crafted extraction rules, limiting its ability to capture complex patterns from large-scale datasets, and still depends on downstream optimization algorithms to properly incorporate GPR rules. To overcome these limita-

tions, *DeepGDel* [21] was introduced as the first framework to formulate gene deletion strategy design as a predictive learning task using deep learning techniques [22], laying the foundation for fully data-driven gene deletion strategy design. *DeepGDel* jointly models gene and metabolite sequences along with existing gene deletion strategy data, enabling end-to-end prediction of growth-coupled gene deletion strategies and demonstrating robust applicability across metabolic models from diverse species and scales. Although *DeepGDel* effectively models metabolite features from sequential input data, it ignores upstream and downstream interactions that are widely recognized as essential for understanding the complexity of metabolic systems [23], [24], [25]. This limitation reduces predictive performance, particularly on large genome-scale models. Graph-based representations provide a natural framework for capturing such structured dependencies and offer critical context for understanding the coupling between target metabolite production and cell growth. Recent advances in graph learning have demonstrated strong potential for extracting meaningful relationships from graph-structured biological data, enabling effective solutions across diverse biological tasks [26], [27], [28]. Based on these observations, integrating graph-based learning into gene deletion strategy design to better capture metabolite interactions is highly desirable.

However, achieving this goal is not straightforward. Unlike curated pathway maps, such as those provided by KEGG (Kyoto Encyclopedia of Genes and Genomes) [29], genome-scale metabolic models do not explicitly define topological relationships among biological entities in the form of a graph [30], [31]. Instead, they rely on algebraic representations: stoichiometric matrices encoding mass-balance constraints, Boolean expressions defining GPR rules, and flux bounds specified as interval constraints. Since these formulations are inherently algebraic rather than topological, they lack an explicit graph structure in which nodes represent biological entities and edges represent their interactions. This absence of graph structure hinders the direct application of metabolic models in graph-based computation and learning. Moreover, there is a central challenge in constructing meaningful graph representations from metabolic models: the treatment of ubiquitous metabolites, such as ATP, NAD(H), and other common cofactors that participate in a wide range of reactions. These metabolite act as topological hubs, often obscuring the modular organization of metabolic networks and diluting biologically meaningful structures [32], [25]. Although such entities are commonly collapsed or excluded in databases like KEGG and BiGG to improve visual clarity, their impact on graph-based learning remains underexplored and poorly understood [33].

To address the aforementioned challenges, this work aims to achieve two primary objectives. First, we propose a systematic approach to **construct graph representations** from input constraint-based metabolic models. This construction process incorporates two core refinement steps. The graph attribute-based refinement focuses on filtering and removing highly connected nodes, while the knowledge-based refinement targets the editing of currency metabolite nodes, thereby producing graphs that are both biologically grounded and informative. Second, we introduce *GraphGDel*, a deep learning framework that learning from both sequence data and constructed metabolic graphs. *GraphGDel* consists of four neural network-based modules: (1) **Gene-M**, a sequence learning module that encodes gene inputs; (2) **Meta-M**, a sequence learning module that encodes metabolite inputs; (3) **Graph-M**, a graph learning

module that further captures metabolite interactions within the metabolic model; and (4) **Pred-M**, a prediction module that integrates upstream representations to predict growth-coupled gene deletion strategies in genome-scale metabolic models.

To the best of our knowledge, this is the first study to explore graph learning in the context of gene deletion strategy prediction. Computational experiments demonstrated that the graphs constructed by the proposed method are topologically simplified yet remain well-suited for graph-based learning tasks on genome-scale metabolic models. Furthermore, the proposed framework, *GraphGDel*, effectively predicted gene deletion strategies for growth-coupled production across three metabolic models in a fully data-driven manner, achieving robust performance and outperforming baseline methods in overall accuracy, macro-averaged precision, recall, F1 score, and AUC.

The remaining sections of this paper are organized as follows: Section II-A and Section II-B formalize the fundamental concepts used in this study and illustrate them with a small example. Section III presents (1) the proposed approach for constructing graph representations from constraint-based metabolic models, and (2) the proposed *GraphGDel* framework together with its implementation details. Section IV-A outlines the setup of the computational experiments. Sections IV-B, IV-C, IV-D, and IV-E describe the datasets, baseline methods, and evaluation metrics. Section IV-F discusses the experimental results, including: (1) performance comparisons between the proposed framework and baseline methods; (2) comparisons of *GraphGDel* ablation variants that use different learning modules; and (3) comparisons of *GraphGDel* variants using different metabolic graph representations across the *e_coli_core*, *iMM904*, and *iML1515* models. Finally, Section V analyzes the results, evaluates the performance of *GraphGDel* and its variants, and discusses limitations and directions for future work.

II. PRELIMINARY AND PROBLEM SETTING

In this section, we first outline several key terms in this study as a preliminary. Next, we illustrate these concepts using a toy constraint-based model. Finally, we define the main problem in this research, namely, **gene deletion strategy prediction**. All the notations mentioned in this section are listed in Table I.

A. Preliminary Definition

1) **Constraint-based model**: Let $\mathcal{C} = \{M, R, S, L, U, G, F, P\}$ be a constraint-based model. The elements of \mathcal{C} can be further divided into two parts: (1) the metabolic network and (2) the GPR rule. We describe them as follows:

- **Metabolic network**: Let $\mathcal{C}_1 = \{M, R, S, L, U\}$ be a metabolic network. $M = \{m_1, \dots, m_{|M|}\}$ denotes a set consisting all metabolites, with one of them being the target metabolite m_{target} . $R = \{r_1, \dots, r_{|R|}\}$ denotes a set consisting all reactions, including the cell growth reaction r_{growth} and the target metabolite production reaction r_{target} . To facilitate clarity, we introduce an additional set $V = \{v_1, \dots, v_{|R|}\}$ to represent the reaction rates per unit time (flux) corresponding to reactions in R . Notably, we distinguish the rate of the growth reaction (v_{growth}) as the **Growth Rate (GR)** and that of the target metabolite production reaction (v_{target}) as the **Production Rate (PR)**. The stoichiometry matrix S contains elements $S_{ij} = k$, indicating that reaction

TABLE I: Notations used in the definitions in preliminary and problem setting.

Notation	Description
\mathcal{C}	Constraint-based model
\mathcal{C}_1	Metabolic network
\mathcal{C}_2	GPR rule
M	Metabolites in the constraint-based model
R	Reactions in the constraint-based model
V	Reaction rates (flux)
S	Stoichiometry matrix
L	Lower bounds for reaction rates
U	Upper bounds for reaction rates
G	Genes in the constraint-based model
F	Boolean functions for GPR rule
P	Outputs of Boolean functions in F
m_{target}	Target metabolite
r_{target}	Target metabolite production reaction
r_{growth}	Cell growth reaction
$PR_{\text{threshold}}$	Minimum requirement for target production reaction rate
$GR_{\text{threshold}}$	Minimum requirement for cell growth reaction rate
G_{del}	Genes deleted in the gene deletion strategy
DS	Set of gene deletion strategies
DS_{known}	Set of known gene deletion strategies
\bar{DS}	Predicted gene deletion strategies
DS^*	Ground-truth strategies corresponding to \bar{DS}
$\mathcal{F}(\theta)$	Predictive model parameterized by θ

r_j either produces (+) or consumes (-) k units of metabolite m_i per unit time. Lower and upper bounds for the reaction rates for V are denoted by $L = \{l_1, \dots, l_{|R|}\}$ and $U = \{u_1, \dots, u_{|R|}\}$, respectively.

• **GPR rule:** Let $\mathcal{C}_2 = \{G, F, P\}$ be a GPR rule. $G = \{g_1, \dots, g_{|G|}\}$ represents a set of genes, while $F = \{f_1, \dots, f_{|R|}\}$ represents Boolean functions. $P = \{p_1, \dots, p_{|R|}\}$ is a collection of outputs generated by applying the functions in F to the gene set G . Each output p_j can be expressed as $p_j = f_j(G)$, where both p and g are binary values, i.e., $p, g \in \{0, 1\}$. Note that if $p_j = 0$, this imposes a constraint on both the lower bound l_j and the upper bound u_j to be 0, effectively restraining reaction r_j .

2) **Flux balance analysis:** When analyzing a metabolic network within a constraint-based model, flux balance analysis (FBA) assumes a steady state in which all metabolic reaction fluxes remain constant [30]. Formally, FBA imposes the following conditions: (1) for each metabolite, the sum of producing fluxes equals the sum of consuming fluxes; (2) in each reaction, substrate and product fluxes must satisfy the stoichiometric ratios specified by the reaction equation; and (3) each flux is constrained by prescribed upper and lower bounds. In the standard formulation of FBA applied to a metabolic network \mathcal{C}_1 , the objective is to maximize the cell growth reaction rate v_{growth} , expressed as the following linear program (LP):

LP Formalization of FBA Using \mathcal{C}_1 of a Constraint-Based Model.

Given: \mathcal{C}_1

Maximize: v_{growth}

Such that:

$$\begin{aligned} \sum_j S_{ij} v_j &= 0 \quad \text{for all } i; \\ l_j \leq v_j \leq u_j &\quad \text{for all } j; \\ i &= \{1, \dots, |M|\}, \quad j = \{1, \dots, |R|\} \end{aligned}$$

3) **Growth-coupled production:** Growth-coupled production is a special case of microbial metabolism, wherein cell growth co-occurs with the synthesis of a target metabolite. In

this study, we adopt the paradigm of *weakly growth-coupled production*, which requires achieving a non-zero synthesis rate of the target metabolite at the maximum non-zero growth rate [34], [35]. During the simulation of constraint-based models, growth-coupled production can be characterized by two indices: the lower bound of the target metabolite production rate ($PR_{\text{threshold}}$) and the lower bound of the cell growth reaction rate ($GR_{\text{threshold}}$). When the growth rate is maximized, if the simulated values v_{growth} and minimum v_{target} exceed their respective lower bounds, growth-coupled production is considered to be achieved. In this study, we set $PR_{\text{threshold}} = GR_{\text{threshold}} = 0.001$.

4) **Gene deletion strategy:** In metabolic model simulations, a gene deletion strategy refers to selecting genes for removal in order to optimize the network toward desired outcomes, such as the growth-coupled production of specific metabolites. For growth-coupled production, the gene deletion strategy is typically formulated as identifying a set G_{del} of genes designated for deletion, as follows:

Calculation of Gene Deletion Strategy for Growth-Coupled Production.

Given: \mathcal{C} , r_{target} , $PR_{\text{threshold}}$, $GR_{\text{threshold}}$

Find: $G_{\text{del}} \subset G$ such that $v_{\text{target}} \geq PR_{\text{threshold}}$ and $v_{\text{growth}} \geq GR_{\text{threshold}}$

Such that Minimize:

$$v_{\text{target}}$$

Such that Maximize:

$$v_{\text{growth}}$$

Such that:

$$\begin{aligned} \sum_j S_{ij} v_j &= 0 \quad \text{for all } i; \\ \begin{cases} v_j = 0 & \text{if } p_j = 0, \\ l_j \leq v_j \leq u_j & \text{otherwise;} \end{cases} \\ p_j &= f_j(G); \\ \begin{cases} g = 0 & \text{if } g \in G_{\text{del}}, \\ g = 1 & \text{otherwise;} \end{cases} \end{aligned}$$

B. Example: Gene Deletions in Metabolic Models

A small example with accompanying explanations is provided below to further illustrate gene deletions in metabolic models.

1) **Toy constraint-based model setup:** Fig. 1 shows a toy example in which $\mathcal{C} = \{M, R, S, L, U, G, F, P\}$ represents a constraint-based model. Specifically, for its metabolic network part \mathcal{C}_1 , we have $M = \{m_1, \dots, m_5\}$, $R = \{r_1, \dots, r_8\}$, $S = \begin{pmatrix} 1 & 0 & -1 & -1 & 0 & 0 & 0 & 0 \\ 0 & 1 & 0 & 0 & -1 & 0 & 0 & 0 \\ 0 & 0 & 1 & 0 & 0 & -1 & 0 & 0 \\ 0 & 0 & 0 & 0 & 1 & 1 & -1 & 0 \\ 0 & 0 & 0 & 1 & 0 & 1 & 0 & -1 \end{pmatrix}$, $L = \{0, 0, 0, 0, 0, 0, 0, 0\}$, and $U = \{10, 10, 5, 10, 10, 5, 10, 10\}$. For its gene reaction rule part \mathcal{C}_2 , we have $G = \{g_1, \dots, g_8\}$, $F = \{f_1, \dots, f_8\}$, and $P =$

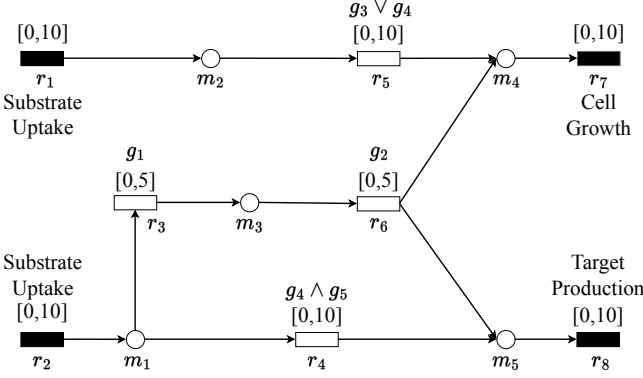


Fig. 1: A toy example of the constraint-based model where circles and rectangles represent metabolites and reactions, respectively. Black and white rectangles denote external and internal reactions, respectively. r_1, r_2 correspond to two substrate uptake reactions. r_7, r_8 correspond to cell growth, and target metabolite production reactions, respectively. The reaction rates are constrained by the range $[l_i, u_i]$. In this example, all stoichiometric ratios are 1 or -1.

TABLE II: Gene deletion strategies for the toy example in Fig. 1 are classified into five types based on the resulting flux (reaction rate) distributions.

Type	Gene deletion strategies classified by flux distributions
1	$\emptyset, \{g_1\}, \{g_2\}, \{g_3\}, \{g_1, g_2\}, \{g_1, g_3\}, \{g_2, g_3\}, \{g_1, g_2, g_3\}$
2	$\{g_4\}, \{g_5\}, \{g_3, g_5\}, \{g_4, g_5\}$
3	$\{g_1, g_4\}, \{g_2, g_4\}, \{g_1, g_2, g_4\}, \{g_1, g_5\}, \{g_2, g_4\}, \{g_1, g_2, g_5\}, \{g_1, g_3, g_5\}, \{g_1, g_4, g_5\}, \{g_2, g_3, g_5\}, \{g_2, g_4, g_5\}, \{g_1, g_2, g_3, g_5\}, \{g_1, g_2, g_4, g_5\}$
4	$\{g_3, g_4\}, \{g_3, g_4, g_5\}$
5	$\{g_1, g_3, g_4\}, \{g_2, g_3, g_4\}, \{g_1, g_2, g_3, g_4\}, \{g_1, g_3, g_4, g_5\}, \{g_2, g_3, g_4, g_5\}, \{g_1, g_2, g_3, g_4, g_5\}$

$\{p_1, \dots, p_8\}$, where

$$f_i : p_i = \begin{cases} 1, & i = 1 \\ 1, & i = 2 \\ g_1, & i = 3 \\ g_4 \wedge g_5, & i = 4 \\ g_3 \vee g_4, & i = 5 \\ g_2, & i = 6 \\ 1, & i = 7 \\ 1, & i = 8 \end{cases}$$

In this toy model \mathcal{C} , the gene-reaction rule for r_4 is given as $f_4 : p_4 = g_4 \wedge g_5$. Thus, the reaction rate of r_4 (denoted v_4) is forced to be 0 if either g_4 or g_5 is 0 (deleted). If both g_4 and g_5 are 1 (not deleted), then $0 \leq v_4 \leq 10$. For r_5 , the reaction rate v_5 is forced to be 0 only if both g_3 and g_4 are 0. If at least one of g_3 or g_4 is 1, then $0 \leq v_5 \leq 10$. For r_1, r_2, r_7 , and r_8 , since $p_1 = p_2 = p_7 = p_8 = 1$ always holds, none of v_1, v_2, v_7 , or v_8 can be forced to 0 by any gene deletions.

In this example, m_5 is designated as the target metabolite, produced through the target metabolite production reaction r_8 .

2) **Gene deletions on the toy constraint-based model:** Table II describes the patterns of gene deletions in this example: the $2^5 = 32$ patterns are classified into five types based on the flux distributions. The detailed flux distributions for all types can

TABLE III: The resulting flux distributions for gene deletion strategy Types 1 to 5. For each type, the most optimistic (best) and pessimistic (worst) target metabolite production rate (PR, v_8) at cell growth rate (GR, v_7) maximization are provided.

ID	Deletion strategy	PR situation	Flux distribution							
			v_1	v_2	v_3	v_4	v_5	v_6	v_7	v_8
1	Type 1	best	10	10	0	10	10	0	10	10
2		worst	10	0	0	0	10	0	10	0
3	Type 2	best	5	5	5	0	5	5	5	5
4		worst	10	0	0	0	10	0	10	0
5	Type 3	best	10	0	0	0	10	0	10	0
6		worst	10	0	0	0	10	0	10	0
7	Type 4	best	0	5	5	0	0	5	5	5
8		worst	0	5	5	0	0	5	5	5
9	Type 5	best	0	0	0	0	0	0	0	0
10		worst	0	0	0	0	0	0	0	0

be found in Table III.

In the original toy model without gene deletions, two paths lead to cell growth (r_7): $r_1 \rightarrow r_5 \rightarrow r_7$ and $r_2 \rightarrow r_3 \rightarrow r_6 \rightarrow r_7$. Two paths from r_2 reach the target production reaction (r_8): $r_2 \rightarrow r_3 \rightarrow r_6 \rightarrow r_8$ and $r_2 \rightarrow r_4 \rightarrow r_8$. A maximal growth rate of $GR = 10$ is achievable, but the flux distribution is not unique.

If both the path leading to cell growth ($r_1 \rightarrow r_5 \rightarrow r_7$) and the path leading to target production ($r_2 \rightarrow r_4 \rightarrow r_8$) are used at maximum flux, then $GR = 10$ and $PR = 10$ are obtained, as shown in the flux distribution of ID 1 in Table III. This represents the most optimistic case for the flux value of PR. In contrast, if only the path ($r_1 \rightarrow r_5 \rightarrow r_7$) is used at maximum flux, then $GR = 10$ and $PR = 0$ are obtained, as shown in the flux distribution of ID 2 in Table III. This represents the most pessimistic case for the flux value of PR. As previously defined, in the context of growth-coupled production, we evaluate PR in the most pessimistic case when GR is maximized. Therefore, in the original state of the toy model, we have $GR = 10$ and $PR = 0$. We denote this flux distribution as Type 1. Seven gene deletion strategies, $\{g_1\}, \{g_2\}, \{g_3\}, \{g_1, g_2\}, \{g_1, g_3\}, \{g_2, g_3\}$, and $\{g_1, g_2, g_3\}$, are also classified as Type 1, as they yield the same flux distribution.

IDs 3 and 4 in Table III describe the most optimistic and pessimistic flux distributions with respect to PR when g_4 is deleted. Deleting g_4 gives $f_4 : p_4 = g_4 \wedge g_5 = 0$, forcing $v_4 = 0$. The maximal growth rate is $GR = 10$, since all paths to the growth reaction r_7 (from r_1 or r_2 to r_7) remain available. In the most optimistic case, both the path $r_1 \rightarrow r_5 \rightarrow r_7$ and the path $r_2 \rightarrow r_3 \rightarrow r_6 \rightarrow r_7$ are used, with the latter achieving maximal flux, resulting in $GR = 10$ and $PR = 5$. In the most pessimistic case, only the first path is used at maximal flux, giving $GR = 10$ and $PR = 0$. We denote this flux distribution as Type 2. The gene deletion strategies $\{g_5\}, \{g_3, g_5\}$, and $\{g_4, g_5\}$ are also classified as Type 2, as shown in Table III.

IDs 5 and 6 in Table III describe the flux distributions when g_1 and g_4 are deleted. In this case, $f_3 : p_3 = g_1 = 0$ and $f_4 : p_4 = g_4 \wedge g_5 = 0$, forcing $v_3 = 0$ and $v_4 = 0$. The maximal growth rate is $GR = 10$, since the path $r_1 \rightarrow r_5 \rightarrow r_7$ remains available. This yields a uniquely determined flux distribution with $v_1 = v_5 = 10$ and $v_2 = v_3 = v_4 = v_6 = 0$. Consequently, both the optimistic and pessimistic PR values are zero, with $GR = 10$. We denote this flux distribution as Type 3. Eleven additional gene deletion strategies are also classified as Type 3, as shown in Table III.

IDs 7 and 8 in Table III describe the flux distributions when

g_3 and g_4 are deleted. In this case, $f_4 : p_4 = g_4 \wedge g_5 = 0$ and $f_5 : p_5 = g_3 \vee g_4 = 0$, forcing $v_4 = 0$ and $v_5 = 0$. This yields a uniquely determined flux distribution with $v_2 = v_3 = v_6 = 4$ and $v_1 = v_4 = v_5 = 0$. Consequently, both the optimistic and pessimistic PR values are 5, with maximal $GR = 5$. We denote this flux distribution as Type 4. Another gene deletion strategy, $\{g_3, g_4, g_5\}$, is also classified as Type 4, as shown in Table III.

IDs 9 and 10 in Table III describe the flux distributions when g_1 , g_3 , and g_4 are deleted. In this case, $f_3 : p_3 = g_1 = 0$, $f_4 : p_4 = g_4 \wedge g_5 = 0$, and $f_5 : p_5 = g_3 \vee g_4 = 0$, forcing $v_3 = v_4 = v_5 = 0$. The maximal growth rate is $GR = 0$, as no path to the growth reaction r_7 remains viable. This yields a uniquely determined flux distribution with all reaction fluxes equal to zero, resulting in $PR = 0$ in both the optimistic and pessimistic cases. We denote this flux distribution as Type 5. The gene deletion strategies $\{g_2, g_3, g_4\}$, $\{g_1, g_2, g_3, g_4\}$, $\{g_1, g_3, g_4, g_5\}$, $\{g_2, g_3, g_4, g_5\}$, and $\{g_1, g_2, g_3, g_4, g_5\}$ are also classified as Type 5, as shown in Table III.

Across the five types of gene deletion strategies analyzed above, only Type 4 satisfies $PR \geq PR_{\text{threshold}}$ and $GR \geq GR_{\text{threshold}}$, even in the most pessimistic scenario. Consequently, in this toy model, only the two Type 4 gene deletion strategies, $\{g_3, g_4\}$ and $\{g_3, g_4, g_5\}$, enable growth-coupled production of the target metabolite m_5 .

C. Problem Setting

Gene deletion strategy prediction. Given a constraint-based metabolic model \mathcal{C} and a set of metabolites M , the task of gene deletion strategy prediction seeks to infer the gene deletion strategies DS of target metabolites $M_{\text{target}} \subseteq M$. This task operates under the assumption that gene deletion strategies for a subset of metabolites, denoted as DS_{known} , are already established, while the strategies for the target metabolites remain unknown. The primary objective is to develop a computational agent, such as a predictive model $\mathcal{F}(\theta)$, which processes the known deletion strategies along with the information on the metabolic model. This agent aims to generate predictions \widehat{DS} for the target metabolites, optimizing its outputs to closely approximate the ground-truth deletion strategies DS^* , as presented below:

Prediction of Gene Deletion Strategies for Target Metabolites.

Given: \mathcal{C} , DS_{known}

Objective: A computational agent $\mathcal{F}(\theta)$, parameterized by θ , to generate deletion strategy predictions \widehat{DS} for the target metabolites $M_{\text{target}} \subseteq M$.

Such that:

$$\begin{aligned}\widehat{DS} &= \mathcal{F}(\theta; DS_{\text{known}}, \mathcal{C}); \\ \widehat{DS} &\approx DS^*\end{aligned}$$

III. METHOD

In this section, we first introduce our method for constructing graph representations from input metabolic models. Next, we present the *GraphGDel* framework, outlining its overall design, explaining the structure and function of each module, and describing the specific deep learning models used for predicting gene deletion strategies. Finally, we provide implementation details, including the parameter settings and training procedures of the *GraphGDel* framework.

A. Constructing Graph Representations of Metabolic Models

We present a pipeline for constructing a biologically meaningful graph representation from a genome-scale metabolic model. The process begins by extracting core biochemical entities and their interactions, followed by two refinement steps that incorporate both graph-structural properties and domain-specific metabolite knowledge. The resulting graph preserves essential metabolic structure while reducing confounding topological noise, thereby enabling more interpretable and effective downstream graph-based learning.

The construction procedure consists of the following four steps:

- **Step 1: Construct Temporary Graph from Input Metabolic Model.**

We begin with a genome-scale metabolic model as input. As the metabolic model lacks an explicit topological form, we draft a temporary graph $\mathcal{G}_{\text{temp}}$ from its components. We construct $\mathcal{G}_{\text{temp}}$ as a tripartite heterogeneous graph consisting of three node types: metabolites, reactions, and genes. Directed edges are defined from metabolites to reactions (for substrates), from reactions to metabolites (for products), and from genes to reactions (based on GPR rules). This graph encodes the complete structural and regulatory logic of the metabolic model.

- **Step 2: Induce the Metabolite Graph.**

To focus on metabolite-level connectivity, we remove gene nodes and treat each reaction node in $\mathcal{G}_{\text{temp}}$ as a hyper-edge connecting all its associated metabolites. We then project this hypergraph into a pairwise undirected graph by linking each reactant to each product within the same reaction. The resulting metabolite graph, denoted as \mathcal{G}_0 , contains only metabolite nodes, with edges representing biochemical transformations.

- **Step 3: Graph Attribute-Based Node Filtering.**

Highly connected hub-like metabolites can distort the network's topological structure by disproportionately influencing properties such as shortest paths and information flow. To reduce this topological noise, we identify and remove from \mathcal{G}_0 the ten metabolites with the highest degree, resulting in a trimmed graph \mathcal{G}_1 .

- **Step 4: Knowledge-Based Node Refinement.**

We apply a two-step refinement process to enhance biological interpretability, resulting in the final graph $\mathcal{G}_{\text{final}}$: **(1) Remove canonical currency metabolites.** We exclude known currency metabolites based on a curated list from KEGG and BiGG databases, including: `["atp", "adp", "amp", "nad", "nadh", "nadp", "nadph", "coa", "h", "h2o", "pi", "ppi", "co2", "nh4", "o2", "glutathione", "na1", "k", "mg2", "ca2"]`.

(2) Selectively restore removed metabolites. Any metabolite removed in previous steps that corresponds to a designated production target (e.g., a growth-coupled product) or a non-currency, high-degree metabolite is selectively reintroduced to maintain the functional integrity of the $\mathcal{G}_{\text{final}}$.

As a result, the proposed graph construction pipeline produces a representation that preserves key functional structures while minimizing the confounding influence of topological hubs. The pseudocode of the proposed graph construction pipeline is presented below:

Constructing Metabolite Graph from a Constraint-Based Metabolic Model

Input: $\mathcal{C} = \{M, R, S, G, F\}$ where:

- $M = \{m_1, \dots, m_{|M|}\}$: metabolites (including m_{target})
- $R = \{r_1, \dots, r_{|R|}\}$: reactions
- $S \in \mathbb{R}^{|M| \times |R|}$: stoichiometric matrix, where S_{ij} is the coefficient of m_i in r_j
- $G = \{g_1, \dots, g_{|G|}\}$: genes
- $F = \{f_1, \dots, f_{|F|}\}$: GPR Boolean functions mapping subsets of G to reactions

Currency Metabolite Set:

$\mathcal{U} = \{\text{atp}, \text{adp}, \text{amp}, \text{nad}, \text{nadh}, \text{nadp}, \text{nadph}, \text{coa}, \text{h}, \text{h2o}, \text{pi}, \text{ppi}, \text{co2}, \text{nh4}, \text{o2}, \text{glutathione}, \text{na1}, \text{k}, \text{mg2}, \text{ca2}\}$.

Step 1: Construct Temporary Graph from Input Metabolic Model

Define node set:

$$V_{\text{temp}} = M \cup R \cup G$$

Define directed edge set E_{temp} :

- Add (m_i, r_j) if $S_{ij} < 0$ (metabolite is a substrate)
- Add (r_j, m_i) if $S_{ij} > 0$ (metabolite is a product)
- Add (g_k, r_j) if g_k appears in f_j (GPR rule)

Resulting graph:

$$\mathcal{G}_{\text{temp}} = (V_{\text{temp}}, E_{\text{temp}})$$

Step 2: Induce Metabolite Graph \mathcal{G}_0

Project each reaction node into undirected metabolite pairs:

- For each reaction r_j , for every substrate m_i ($S_{ij} < 0$) and every product $m_{i'}$ ($S_{i'j} > 0$), add undirected edge $(m_i, m_{i'})$.

Define metabolite-only graph:

$$\mathcal{G}_0 = (V_0 = M, E_0)$$

Step 3: Graph Attribute-Based Node Filtering

Compute degrees:

$$\deg(m) = |\{v \mid (m, v) \in E_0, m, v \in V_0\}|$$

Select top- k high-degree nodes:

H_k = Top- k metabolites by degree

Remove them:

$$V_1 = V_0 \setminus H_k, \quad E_1 = \{(m_i, m_j) \in E_0 \mid m_i, m_j \in V_1\}$$

$$\mathcal{G}_1 = (V_1, E_1)$$

Step 4: Knowledge-Based Node Refinement

(1) Remove canonical currency metabolites given by \mathcal{U} :

$$V_2 = V_1 \setminus \mathcal{U}, \quad E_2 = \{(m_i, m_j) \in E_1 \mid m_i, m_j \in V_2\}$$

$$\mathcal{G}_2 = (V_2, E_2)$$

(2) Selectively restore removed metabolites:

$$T = \{m \in H_k \mid m = m_{\text{target}} \text{ or } m \notin \mathcal{U}\}$$

$$V_3 = V_2 \cup T$$

$$E_T = \{(m_i, m_j) \in E_0 \mid (m_i \in T \text{ or } m_j \in T) \text{ and } m_i, m_j \in V_3\}$$

$$E_3 = E_2 \cup E_T$$

$$\mathcal{G}_{\text{final}} = (V_3, E_3)$$

Output: Final graph $\mathcal{G}_{\text{final}} = (V_3, E_3)$

B. GraphGDel Framework Overview

Metabolic processes are determined not only by the intrinsic properties of genes and metabolites but also by the complex interactions among metabolites. While sequence information captures molecular-level characteristics of genes and metabolites, it is the upstream and downstream relationships between metabolites that determine how perturbations, such as gene deletions, propagate through the system. Capturing both perspectives is therefore desirable for accurately predicting growth-coupled production outcomes.

To address this, the *GraphGDel* framework integrates sequence learning with graph-based learning to achieve: (1) extraction of gene and metabolite features from sequence data using sequence learning; (2) refinement of metabolite features in the context of the metabolic network using graph-based learning; and (3) integration of sequence- and graph-based features to model gene–metabolite interdependencies for prediction.

Specifically, as illustrated in Fig. 2, *GraphGDel* consists of four neural network modules: the metabolite representation learning module (**Meta-M**), the gene representation learning module (**Gene-M**), the graph representation learning module (**Graph-M**), and the deletion strategy prediction module (**Pred-M**).

- **Meta-M:** This module captures the characteristics of metabolites in the metabolic model. It formulates a metabolite representation learning task that projects input metabolite data into a latent representation, Z_{meta} , summarizing metabolite-relevant information. This unsupervised learning task typically employs a sequence learning model with an autoencoder structure. The learned Z_{meta} serves as a foundation for both downstream graph-based learning and the final gene deletion prediction task.
- **Gene-M:** This module captures the characteristics of genes in the metabolic model. Parallel to Meta-M, it formulates a gene representation learning task that projects input gene data into a latent representation, Z_{gene} , summarizing gene-relevant information. This unsupervised learning task can also employ a sequence learning model with an autoencoder structure. The learned Z_{gene} serves as a foundation for the final gene deletion prediction task.
- **Graph-M:** This module captures the topological relationships and structural patterns within the metabolic graph to refine metabolite features. It formulates a link prediction task that maps the input metabolic graph and metabolite features into a refined latent representation, Z_{metaG} , integrating both metabolite characteristics and their graph connectivity patterns. This unsupervised learning task employs a graph learning model as the encoder and a pairwise node aggregation mechanism as the decoder. The learned Z_{metaG} provides metabolic model-specific information for the final gene deletion prediction task.
- **Pred-M:** This module integrates the latent representations Z_{meta} from Meta-M, Z_{gene} from Gene-M, and Z_{metaG} from Graph-M into a unified latent representation Z , capturing interdependencies between metabolites and genes. The integration process combines sequence-based and graph-based features, transforming them into discriminative features optimized for prediction. Finally, a supervised predictor is trained on Z to infer the deletion status of each gene for different target metabolites within the given metabolic model.

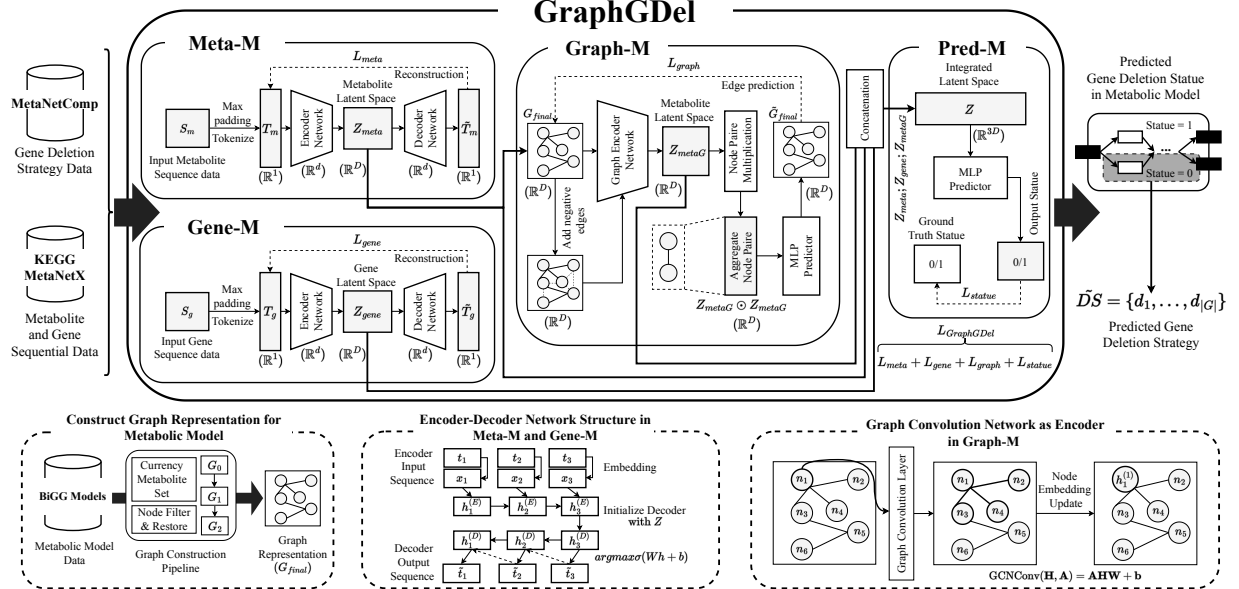


Fig. 2: A system overview of the proposed gene deletion strategy prediction framework. The framework comprises four neural network-based modules: (1) **Meta-M**, which learns the metabolite latent representation Z_{meta} , (2) **Gene-M**, which learns the gene latent representation Z_{gene} , (3) **Graph-M**, which learns the refined metabolite latent representation Z_{metaG} in a specific metabolic graph, and (4) **Pred-M**, which integrates the three upstream latents into a new latent representation, Z , for final gene deletion prediction.

C. Gene Deletion Strategy Prediction

1) **Metabolite Representation Learning:** The Meta-M module is designed to transform raw character strings input, i.e., the SMILES (Simplified Molecular Input Line Entry System) sequences of metabolites into dense, informative feature vectors [36]. To effectively capture the complex patterns within these chemical representations, we employ a sequence-to-sequence autoencoder architecture based on Long Short-Term Memory (LSTM) networks [37], [38]. We selected LSTM as the default model because our goal is to propose a general learning framework for this task and to validate its effectiveness. The LSTM meets these requirements: it is straightforward to implement and provides a strong baseline for future comparisons with more complex replacements, such as Transformer-based models [39].

Given a SMILES sequence S_m of length L_m , the module first performs character-level tokenization to convert the chemical string into a numerical representation suitable for neural network processing. The tokenization process constructs a vocabulary \mathcal{V} from all unique characters appearing in the SMILES dataset, including atomic symbols, bond indicators, and structural notations. Each SMILES sequence $S_m^{(i)}$ is then mapped to a sequence of token indices:

$$\mathbf{T}_m^{(i)} = [t_1, t_2, \dots, t_{L_m}], \quad t_j \in \mathcal{V}, \quad (1)$$

where t_j represents the index of the j -th character in the vocabulary.

To ensure consistent dimensionality across different sequence lengths, we apply zero-padding to standardize all sequences to a maximum length L_{max} :

$$\mathbf{T}_m^{(i)} = [t_1, t_2, \dots, t_{L_m}, 0, 0, \dots, 0], \quad \text{if } L_m < L_{max}. \quad (2)$$

The tokenized sequence is then embedded into a continuous

vector space through a learnable embedding layer:

$$\mathbf{X}_m = \text{Embedding}(\mathbf{T}_m), \quad (3)$$

where the embedding operation maps each token index to a dense vector representation of dimension d .

The embedded sequence is processed through an LSTM encoder that captures the sequential dependencies and chemical patterns within the SMILES string:

$$\mathbf{h}_l = \text{LSTM}(\mathbf{x}_l, \mathbf{h}_{l-1}, \mathbf{c}_{l-1}), \quad (4)$$

where $\mathbf{h}_l \in \mathbb{R}^d$ represents the hidden state at time step l , and \mathbf{c}_l is the cell state that maintains long-term memory.

To stabilize the training process and improve generalization, we apply layer normalization to the LSTM outputs:

$$\mathbf{h}_l^{\text{norm}} = \text{LayerNorm}(\mathbf{h}_l). \quad (5)$$

The final metabolite representation $\mathbf{Z}_{meta} \in \mathbb{R}^D$ is obtained through temporal pooling of the normalized hidden states:

$$\mathbf{Z}_{meta} = \frac{1}{L_m} \sum_{l=1}^{L_m} \mathbf{h}_l^{\text{norm}}. \quad (6)$$

To enable unsupervised learning, the module includes a decoder component that reconstructs the original SMILES sequence from the learned representation. The decoder employs an LSTM network that takes the encoded representation \mathbf{Z}_{meta} as input and generates a sequence of token predictions:

$$\tilde{\mathbf{T}}_m = \text{Decoder}(\mathbf{Z}_{meta}). \quad (7)$$

The training objective for Meta-M combines reconstruction loss with representation learning:

$$\mathcal{L}_{meta} = \frac{1}{L_m} \sum_{l=1}^{L_m} \text{CrossEntropy}(\tilde{\mathbf{t}}_l, \mathbf{t}_l), \quad (8)$$

where t_l and \tilde{t}_l are the ground-truth and predicted tokens at position l , respectively.

Through this autoencoder architecture, Meta-M learns to capture the fundamental chemical characteristics of metabolites such as functional groups and structural patterns, resulting in a compact representation $\mathbf{Z}_{\text{meta}} \in \mathbb{R}^D$ that preserves the molecular information necessary for downstream graph-based learning and prediction tasks.

2) **Gene Representation Learning:** The Gene-M module employs an identical neural network architecture to Meta-M, but processes gene sequences represented as amino acid sequences instead of SMILES strings.

Given a gene sequence input \mathbf{S}_g of length L_g , the module follows the same processing pipeline as Meta-M:

$$\mathbf{T}_g^{(i)} = [t_1, t_2, \dots, t_{L_g}], \quad t_j \in \mathcal{V}_g, \quad (9)$$

where \mathcal{V}_g contains the 20 standard amino acid characters and any additional symbols.

The identical LSTM autoencoder architecture processes the amino acid sequence through the following network layers:

$$\left\{ \begin{array}{l} \mathbf{x}_g = \text{Embedding}(\mathbf{T}_g), \\ \mathbf{h}_l = \text{LSTM}(\mathbf{x}_l, \mathbf{h}_{l-1}, \mathbf{c}_{l-1}), \\ \mathbf{h}_l^{\text{norm}} = \text{LayerNorm}(\mathbf{h}_l), \\ \mathbf{Z}_{\text{gene}} \in \mathbb{R}^D = \frac{1}{L_g} \sum_{l=1}^{L_g} \mathbf{h}_l^{\text{norm}}, \\ \tilde{\mathbf{T}}_g = \text{Decoder}(\mathbf{Z}_{\text{gene}}), \end{array} \right. \quad (10)$$

The training objective follows the same reconstruction loss formulation:

$$\mathcal{L}_{\text{gene}} = \frac{1}{L_g} \sum_{l=1}^{L_g} \text{CrossEntropy}(\tilde{t}_l, t_l), \quad (11)$$

where the LSTM is trained to extract informative patterns from amino acid sequences.

This parallel design ensures balanced feature extraction from both biological entities, providing a unified foundation for the subsequent integration in the prediction module.

3) **Graph Representation Learning:** To capture the topological relationships and structural patterns within the metabolic network, we design Graph-M, which employs Graph Convolutional Networks (GCN) to refine the metabolite representations learned by Meta-M in the context of the metabolic network structure. This module takes the sequence-based metabolite features from Meta-M as initial node embeddings and further enhances them by incorporating the graph connectivity patterns through graph convolutions.

Given a metabolic graph $\mathcal{G} = (V, E)$ where V represents the set of metabolite nodes and E represents the set of edges connecting metabolites through reactions, Graph-M processes the graph structure using the Meta-M learned features as initial node representations. Specifically, for each metabolite node $v_i \in V$, we initialize its node features using the corresponding Meta-M representation $\mathbf{Z}_{\text{meta}}^{(i)} \in \mathbb{R}^D$.

The initial node feature matrix $\mathbf{X} \in \mathbb{R}^{|V| \times D}$ is constructed by aggregating the Meta-M representations for all metabolites:

$$\mathbf{X} = [\mathbf{Z}_{\text{meta}}^{(1)}, \mathbf{Z}_{\text{meta}}^{(2)}, \dots, \mathbf{Z}_{\text{meta}}^{(|V|)}]^T, \quad (12)$$

where each row \mathbf{X}_i corresponds to the Meta-M learned representation of metabolite v_i .

To enhance the node features with structural information, we add learnable positional embeddings that capture node identity within the graph:

$$\mathbf{X}_{\text{enhanced}} = \mathbf{X} + \mathbf{P}, \quad (13)$$

where $\mathbf{P} \in \mathbb{R}^{|V| \times d_{\text{pos}}}$ represents learnable positional embeddings for each node, and d_{pos} is the positional embedding dimension.

The enhanced node features are then processed through two graph convolutional layers to capture both local and global structural patterns:

$$\mathbf{H}^{(1)} = \text{ReLU}(\text{GCNConv}(\mathbf{X}_{\text{enhanced}}, \mathbf{A})), \quad (14)$$

$$\mathbf{H}^{(2)} = \text{GCNConv}(\mathbf{H}^{(1)}, \mathbf{A}), \quad (15)$$

where \mathbf{A} is the adjacency matrix of the graph, and $\text{GCNConv}(\cdot, \cdot)$ represents the graph convolutional operation defined as:

$$\text{GCNConv}(\mathbf{H}, \mathbf{A}) = \mathbf{A} \mathbf{H} \mathbf{W} + \mathbf{b}, \quad (16)$$

where \mathbf{W} and \mathbf{b} are learnable weight matrix and bias vector, respectively.

The final graph-refined metabolite embeddings $\mathbf{Z}_{\text{metaG}} \in \mathbb{R}^{|V| \times D}$ are obtained from the second graph convolutional layer:

$$\mathbf{Z}_{\text{metaG}} = \mathbf{H}^{(2)}. \quad (17)$$

To train the Graph-M module, we employ a link prediction task that predicts the existence of edges between node pairs. For a given node pair (i, j) , we compute the link prediction score as:

$$s_{ij} = \sigma(\mathbf{W}_{\text{link}}[\mathbf{Z}_{\text{metaG}}^{(i)} \parallel \mathbf{Z}_{\text{metaG}}^{(j)}] + \mathbf{b}_{\text{link}}), \quad (18)$$

where \parallel denotes concatenation, \mathbf{W}_{link} and \mathbf{b}_{link} are learnable parameters, and $\sigma(\cdot)$ is the sigmoid activation function.

The training objective for Graph-M is the binary cross-entropy loss for link prediction:

$$\mathcal{L}_{\text{graph}} = - \sum_{(i,j) \in E} \log(s_{ij}) - \sum_{(i,j) \notin E} \log(1 - s_{ij}), \quad (19)$$

where the first term corresponds to positive edges (existing connections) and the second term corresponds to negative edges (non-existing connections).

By minimizing this loss, Graph-M learns to refine the Meta-M learned metabolite representations by incorporating the topological relationships within the metabolic network. The resulting $\mathbf{Z}_{\text{metaG}}$ provides graph-enhanced metabolite features that combine the intrinsic molecular characteristics captured by Meta-M with the structural context of the metabolic network, thereby offering a more comprehensive representation for the downstream prediction task.

4) **Gene Deletion Status Prediction:** The Pred-M module integrates the learned representations from all three upstream modules to predict gene deletion status. Given the metabolite representation \mathbf{Z}_{meta} from Meta-M, the gene representation \mathbf{Z}_{gene} from Gene-M, and the graph-refined metabolite representation $\mathbf{Z}_{\text{metaG}}$ from Graph-M, the integration process combines these features to create a unified representation for prediction.

For a specific gene-metabolite pair, we select the corresponding metabolite node from the graph embeddings:

$$\mathbf{Z}_{\text{metaG}}^{(m)} = \mathbf{Z}_{\text{metaG}}[m], \quad (20)$$

where m is the index of the target metabolite in the graph.

The three representations are then concatenated to form a combined feature vector:

$$\mathbf{Z} = [\mathbf{Z}_{\text{meta}} \parallel \mathbf{Z}_{\text{gene}} \parallel \mathbf{Z}_{\text{metaG}}^{(m)}], \quad (21)$$

where \parallel denotes concatenation, resulting in a feature vector of dimension $3D$.

The combined representation is then processed through a fully connected layer followed by a sigmoid activation to produce the final prediction:

$$\hat{y} = \sigma(\mathbf{W}_{\text{pred}} \mathbf{Z} + \mathbf{b}_{\text{pred}}), \quad (22)$$

where $\mathbf{W}_{\text{pred}} \in \mathbb{R}^{1 \times 3D}$ and $\mathbf{b}_{\text{pred}} \in \mathbb{R}$ are learnable parameters, and $\sigma(\cdot)$ is the sigmoid activation function.

The output $\hat{y} \in [0, 1]$ represents the probability that the gene should be deleted (when \hat{y} is close to 0) or retained (when \hat{y} is close to 1) for the given metabolite.

The training objective for the prediction task is the binary cross-entropy loss:

$$\mathcal{L}_{\text{pred}} = -y \log(\hat{y}) - (1 - y) \log(1 - \hat{y}), \quad (23)$$

where $y \in \{0, 1\}$ is the ground-truth label indicating whether the gene should be deleted (0) or retained (1).

The overall training objective for the entire *GraphGDel* framework combines all four loss components:

$$\mathcal{L}_{\text{total}} = \mathcal{L}_{\text{meta}} + \mathcal{L}_{\text{gene}} + \mathcal{L}_{\text{graph}} + \mathcal{L}_{\text{pred}}. \quad (24)$$

This multi-task learning approach ensures that each module learns meaningful representations while contributing to the final prediction task. The framework is trained end-to-end, allowing the representations from each module to be optimized jointly for the gene deletion prediction task.

D. Implementation Details and Model Training

1) *Device*: All neural network models were trained within the proposed framework on an NVIDIA A100-PCIE-40GB GPU with a Xeon Gold 6258R CPU. Model parameters were optimized for 100 epochs using the Adam optimizer with a learning rate of 1×10^{-3} .

2) *Data Partitioning Strategy*: We partitioned the dataset into 90% for training/validation and 10% as an independent test set for final evaluation. Within the training/validation portion, we applied 10-fold stratified splitting. In each fold, approximately 90% of metabolites were used for training and 10% for validation. After selecting the best configuration from the hyperparameter search (see Section III-D3), we retrained the model on the entire training/validation set and evaluated it once on the independent test set. All reported performance metrics are given as the mean and standard deviation across cross-validation folds.

3) *Hyperparameters*: Hyperparameters were tuned via grid search on the training/validation data using 10-fold stratified cross-validation, repeated five times with different random seeds, to identify the optimal configuration, as summarized in Table IV. The configuration with the highest average validation performance across folds was selected, and the corresponding values were used as the default settings of the proposed framework.

4) *Computational Complexity and Runtime*: The computational complexity of the *GraphGDel* framework is dominated by three components: LSTM autoencoders for sequence processing, GCNs for graph learning, and the combined prediction module.

TABLE IV: Grid search for hyperparameter selection. The optimal values are highlighted in underline.

Hyperparameter	Search Space
Embedding dimension (\mathbb{R}^d)	$\{16, \underline{32}, 64, 128\}$
LSTM hidden dimension	$\{16, 32, \underline{64}, 128\}$
LSTM output dimension (\mathbb{R}^D)	$\{16, 32, \underline{64}, 128\}$
GCN hidden channels	$\{32, \underline{64}, 128, 256\}$
GCN output channels (\mathbb{R}^D)	$\{32, \underline{64}, 128, 256\}$
Learning rate	$\{0.0001, \underline{0.001}, 0.01\}$
Batch size	$\{4, \underline{8}, 16, 32\}$
Dropout rate	$\{0.1, \underline{0.2}, 0.3\}$
Positional embedding dimension	$\{8, \underline{16}, 32\}$

For LSTM autoencoders in Meta-M and Gene-M modules, the complexity is $\mathcal{O}(L \cdot d \cdot D)$ per layer, where L is sequence length, d is embedding dimension, and D is hidden dimension. The Graph-M module has complexity $\mathcal{O}(|E| \cdot D)$ per GCN layer for a graph with $|E|$ edges. The overall computational complexity for batch size B is:

$$\mathcal{O}(B \cdot (L_g + L_m) \cdot d \cdot D + B \cdot |E| \cdot D + B \cdot 3D). \quad (25)$$

Empirically, the framework completes 100 epochs in approximately 10 hours under our experimental conditions, with training time varying based on metabolic model size.

IV. COMPUTATIONAL EXPERIMENTS

In this section, we first provide an overview of our design for computational experiments on metabolic models. Next, we describe the experimental setup in detail, including the data, baseline methods, and evaluation metrics employed. Finally, we present the experimental results along with key observations.

A. Overview

In the computational experiments, we consider three metabolic models: *e_coli_core*, *iMM904*, and *iML1515*:

- *e_coli_core* [40] is a simplified metabolic model of *Escherichia coli* (E. coli) that captures only the essential pathways necessary for core metabolic functions. It is widely used for foundational studies of bacterial metabolism and gene interactions.
- *iMM904* [41] is a more comprehensive model of *Saccharomyces cerevisiae* (yeast), incorporating a larger set of reactions and metabolites. It is commonly used for analyzing complex eukaryotic metabolic networks.
- *iML1515* [42] is one of the most detailed metabolic models of E. coli, covering a vast array of metabolic reactions and pathways. It provides a more intricate network compared to *e_coli_core* and is widely used as a genome-scale model for simulations.

We further define several key terms employed in our computational experiments as follows:

- **Growth-essential genes**: These are genes whose deletion results in a maximum GR of zero during FBA. They are crucial for cell growth and should not be deleted when aiming for growth-coupled production.
- **Pre-determined genes**: A gene is defined as pre-determined if its deletion state is consistent (either deleted or non-deleted) for more than 95% of metabolites within

TABLE V: Summary of constraint-based metabolic models used in the computational experiments.

Metabolic model	<i>e_coli_core</i>	<i>iMM904</i>	<i>iML1515</i>
#Genes	137	905	1516
#Growth essential genes	7	110	196
#Pre-determined genes	71	850	1483
#Metabolites	72	1226	1877
#GCP-possible metabolites	48	782	1085
#Reactions	95	1577	2712

the metabolic model. Such genes' deletion states are considered stable and will not be included in the evaluation.

- **GCP-possible metabolites:** These metabolites are theoretically capable of achieving growth-coupled production within the metabolic models. Only GCP-possible metabolites are considered suitable for targeting when calculating gene deletion strategies.

The detailed breakdown of genes, metabolites, and reactions in the studied models is summarized in Table V.

To evaluate the effectiveness and robustness of the proposed framework for graph representation construction and gene deletion strategy prediction, we design three computational experiments on the aforementioned metabolic models:

- 1) **Performance Evaluation:** We assess gene deletion strategy prediction methods, including the proposed method and baseline approaches, on gene deletion strategy prediction tasks. All methods are applied to the three metabolic models, and results are reported separately for each model.
- 2) **Modules Ablation:** We investigate the contribution of different learning modules by selectively removing specific components from the proposed framework. Two ablation variants, Ge-SMILES (using only Gene-M and Meta-M) and Ge-Graph (using only Gene-M and Graph-M), are evaluated across the three metabolic models, with results reported separately for each model.
- 3) **Graph Representation Evaluation:** We assess the impact of different graph representations on the proposed framework for gene deletion strategy prediction. Two graph representations, \mathcal{G}_0 and \mathcal{G}_1 (introduced in Section III-A), generated during the early stages of the graph construction pipeline, are used as input to the learning model. Experiments are conducted on the three metabolic models, with results reported separately for each model.

B. Data and Preprocessing

For the experiments, we use data from four categories associated with each metabolic model: (1) gene deletion strategy data, which serves as the ground truth for prediction tasks; (2) SMILES data, providing information on the metabolites in the models; (3) amino acid (AA) sequence data, providing information on the genes, specifically their encoded proteins in the models; and (4) the metabolite network structure.

1) **Gene Deletion Strategy Data: Description.** In this study, gene deletion strategy data are represented as binary sequences that encode deletion strategies for specific metabolites. Specifically, the gene deletion strategy data $DS = (d_1, \dots, d_{|G|})$ is a binary sequence of length $|G|$, where $|G|$ is the number of genes in the metabolic model, and each element $d_i \in \{0, 1\}$ indicates the state of gene i : $d_i = 0$ if gene i is deleted, and $d_i = 1$ if it is retained. A single target metabolite may have

multiple deletion strategies, as more than one strategy can achieve growth-coupled production. In this study, we focus on the maximal gene deletion strategy, denoted DS_{\max} , where deleting any additional gene would abolish the growth-coupled production of the metabolite.

Data Source. The gene deletion strategy data used in this study are obtained from the MetNetComp database [19]. MetNetComp curates systematically simulated results derived from constraint-based models and computes growth-coupled gene deletion strategies that are minimal or maximal with respect to the number of deleted genes.

We download all available maximal gene deletion strategy data for the three metabolic models under investigation: *e_coli_core*, *iMM904*, and *iML1515*. The raw data include four types of information: (1) the number of remaining genes, (2) the maximum growth rate, (3) the minimum production rate, and (4) a list of remaining genes. We use only the fourth category, which specifies the genes retained in the maximal gene deletion strategy. Binary gene deletion sequences can be readily derived from this remaining gene list.

2) **SMILES Data: Description.** The SMILES data represent the metabolites in the studied metabolic models. Each SMILES string encodes the chemical structure of a metabolite, including atoms, bonds, and stereochemistry, as a textual sequence of characters and notations. SMILES is widely used for analyzing chemical properties, such as molecular similarity, substructure searches, and cheminformatics-based predictions [43], [44], [45].

Data Source. The SMILES data used in this study is obtained from the MetaNetX database [46]. MetaNetX is an online platform for accessing, analyzing, and manipulating genome-scale metabolic networks and biochemical pathways. It curates information from public repositories to integrate data on metabolites and related reactions across many species.

For all three metabolic models under study, we download SMILES data for metabolites corresponding to those with available gene deletion strategy data. For metabolites lacking corresponding SMILES entries in the database, we use dummy SMILES sequences as placeholders.

3) **Amino Acid Sequence Data: Description.** In metabolic models, gene functions encoded by the GPR rules are ultimately carried out by proteins. Accordingly, we use amino acid (AA) sequences to represent gene information. Each AA sequence corresponds to a protein in the metabolic model and is represented as a linear sequence of amino acids using the standard 20 one-letter amino acid codes. AA sequence data have been widely used to study protein structure and function, including functional annotation, structural prediction, and protein-protein interaction analysis [47], [48], [49].

Data Source. The AA sequence data used in this study is obtained from the KEGG database [29]. KEGG provides comprehensive information on protein-coding genes, their products, and associated metabolic pathways. The AA sequence data in KEGG is curated from publicly available genomic resources and is continuously updated to ensure accuracy and relevance.

We download AA sequence data for all three metabolic models under study, covering all genes in each model. For genes lacking corresponding AA sequences in the database, we use dummy sequences as placeholders.

To mitigate class imbalance between deleted and non-deleted genes, we first applied gene-wise balancing: for genes with both deletion states, an equal number of samples was randomly drawn from each state; otherwise, all available in-

TABLE VI: Summary of constructed datasets for three constraint-based metabolic models.

Metabolic model	<i>e_coli_core</i>	<i>iMM904</i>	<i>iML1515</i>
#Deletion strategies	41	105	443
#Genes per strategy	137	905	1516
#SMILES terms	41	99	425
#Dummy SMILES terms	0	6	18
#AA Seq. terms	136	889	1513
#Dummy AA Seq. terms	1	16	3
#Balanced train/val samples	4932	85070	603368
#Balanced test samples	685	9955	68220

stances were retained. Next, global balancing was performed by downsampling the majority class to match the minority, resulting in a fully balanced training set. Due to metabolite number constraints, the final sample sizes approximate, rather than exactly match, the intended ratios. The details of the constructed datasets for the three metabolic models are summarized in Table VI.

C. Baseline Method: DNN

In the first set of experiments, i.e., performance evaluation of gene deletion strategy prediction methods, we employed a deep learning-based baseline: a Deep Neural Network (DNN) [50] to predict gene deletion status. DNNs are widely used as standard baselines in supervised learning tasks because they can capture non-linear relationships in high-dimensional data, even with relatively simple architectures.

In our case, the DNN baseline takes as input the same tokenized and padded sequences of the gene T_g and the metabolite T_m as used in the proposed framework. Unlike the modular, task-specific architecture of our method, this baseline adopts a simpler design: T_g and T_m are independently mapped to dense vectors through separate embedding layers and then concatenated to form a joint representation following:

$$\begin{aligned} \mathbf{X}_g &= \text{Embedding}(T_g), \\ \mathbf{X}_m &= \text{Embedding}(T_m), \\ \mathbf{X} &= [\mathbf{X}_g; \mathbf{X}_m]. \end{aligned}$$

The concatenated embedding \mathbf{X} is passed through two fully connected layers with ReLU activations, followed by a sigmoid output layer that produces the prediction score:

$$\begin{cases} \mathbf{h}_1 = \text{ReLU}(\mathbf{W}_1 \mathbf{X} + \mathbf{b}_1), \\ \hat{y} = \sigma(\mathbf{W}_2 \mathbf{h}_1 + \mathbf{b}_2), \end{cases} \quad (26)$$

where $\hat{y} = P(y = 1 | T_g, T_m; \theta)$, $y \in \{0, 1\}$ is the ground-truth label (deleted or non-deleted), and $\theta = \{\mathbf{W}_1, \mathbf{W}_2, \mathbf{b}_1, \mathbf{b}_2\}$ denotes the set of learnable parameters. The DNN is trained with the same experimental setup as our proposed framework, using the binary cross-entropy loss defined in Equation 23.

This DNN baseline provides a point of comparison for a naive learnable classifier that does not incorporate any task-specific design. Its performance helps evaluate the necessity of our proposed modular design, which integrates distinct tasks (i.e., representation learning in Gene-M, Meta-M, and Grpah-M) within the framework.

D. Baseline Method: DeepGdel

Besides the DNN baseline, we also employ DeepGdel [21] as an advanced baseline for gene deletion strategy prediction.

DeepGdel extends simple DNN approaches by incorporating sequential learning through LSTM-based autoencoders for both gene and metabolite representations, allowing the model to capture long-range dependencies within the input sequences.

Specifically, DeepGdel learns metabolite and gene representations from SMILES and AA sequences using an encoder-decoder architecture:

$$\begin{aligned} \mathbf{Z}_{\text{meta}} &= \text{LSTM-Encoder}(\mathbf{T}_m), \\ \mathbf{Z}_{\text{gene}} &= \text{LSTM-Encoder}(\mathbf{T}_g), \end{aligned}$$

where \mathbf{Z}_{meta} and \mathbf{Z}_{gene} are the learned latent representations for metabolites and genes, respectively. These representations are integrated via element-wise multiplication:

$$\mathbf{Z} = \mathbf{Z}_{\text{meta}} \odot \mathbf{Z}_{\text{gene}},$$

and passed through a fully connected layer with sigmoid activation for the final prediction:

$$\hat{y} = \sigma(\mathbf{W}\mathbf{Z} + \mathbf{b}),$$

where $\hat{y} = P(y = 1 | T_g, T_m; \theta)$ denotes the probability of gene deletion.

DeepGdel is trained using a multi-task learning objective that combines the reconstruction losses from the autoencoders with the binary classification loss. This baseline provides a more sophisticated comparison, demonstrating the effectiveness of sequential learning approaches and highlighting the additional benefits of incorporating graph structure information in our proposed framework.

E. Evaluation Metrics

We evaluate model performance using four metrics: overall accuracy, macro-averaged precision, recall, and F1 score. Definitions of these metrics are provided below.

Overall Accuracy: Accuracy measures the proportion of correctly classified instances out of the total instances. In our experiments, overall accuracy represents the proportion of genes correctly classified as deleted or non-deleted across all metabolites. It is given by:

$$\text{Overall Accuracy} = \frac{\sum_{m=1}^{|M|} \sum_{i=0}^1 (TP_{m_i} + TN_{m_i})}{|M| \times |G|}$$

Macro-Averaged Precision: Precision measures the proportion of true positive predictions out of all positive predictions for each class. The macro-averaged precision is the average of precision values across both classes (deleted and non-deleted genes) and is calculated as:

$$\text{Macro-Averaged Precision} = \frac{1}{|M|} \sum_{m=1}^{|M|} \frac{1}{2} \sum_{i=0}^1 \frac{TP_{m_i}}{TP_{m_i} + FP_{m_i}}$$

Macro-Averaged Recall: Recall (or sensitivity) measures the proportion of true positives out of all actual positives for each class. The macro-averaged recall is the average of recall values across both classes and is given by:

$$\text{Macro-Averaged Recall} = \frac{1}{|M|} \sum_{m=1}^{|M|} \frac{1}{2} \sum_{i=0}^1 \frac{TP_{m_i}}{TP_{m_i} + FN_{m_i}}$$

Macro-Averaged F1 Score: The F1 score is the harmonic mean of precision and recall for each class. The macro-averaged

F1 score is the average of F1 scores across both classes and is given by:

$$\text{Macro-Averaged F1 Score} = \frac{1}{|M|} \sum_{m=1}^{|M|} \frac{1}{2} \sum_{i=0}^1 2 \cdot \frac{\text{Prec.}_{m_i} \cdot \text{Recall}_{m_i}}{\text{Prec.}_{m_i} + \text{Recall}_{m_i}}$$

Macro-Averaged AUC: The Area Under the Receiver Operating Characteristic Curve (AUC) quantifies the ability of a model to discriminate between the two classes. For each metabolite m , the AUC is computed based on the predicted scores and true labels. It is given by:

$$\text{AUC}_m = \frac{1}{|P_m||N_m|} \sum_{p \in P_m} \sum_{n \in N_m} \left[\mathbb{I}(s_p > s_n) + \frac{1}{2} \mathbb{I}(s_p = s_n) \right],$$

where P_m and N_m are the sets of indices of positive (deleted) and negative (non-deleted) genes for metabolite m , s_p and s_n are the predicted scores (probabilities) for gene p and n , respectively, $\mathbb{I}(\cdot)$ is the indicator function that returns 1 if the condition holds, and 0 otherwise. The macro-averaged AUC is the average of the AUC scores across all metabolites:

$$\text{Macro-Averaged AUC} = \frac{1}{|M|} \sum_{m=1}^{|M|} \text{AUC}_m$$

F. Results and Performance Comparison

The results of the three computational experiments, namely (1) Performance Evaluation, (2) Module Ablation, and (3) Graph Representation Evaluation, are summarized in Tables VII, VIII, and IX, respectively.

Performance Evaluation: Across all metabolic models, *GraphGDel* consistently outperformed the baseline methods in overall accuracy, macro-averaged precision, recall, F1 score, and AUC. Specifically, the overall accuracy of *GraphGDel* was 77.35%, 85.54%, and 73.22% for *e_coli_core*, *iMM904*, and *iML1515*, respectively, representing substantial improvements over DNN (63.31%, 69.28%, 60.04%) and DeepGdel (71.18%, 80.58%, 67.91%). This demonstrates the robustness of *GraphGDel* across models of varying scales.

Modules Ablation: To assess the contributions of the learning modules, we evaluated two variants of *GraphGDel*: Ge-SMILES (using only Gene-M and Meta-M) and Ge-Graph (using only Gene-M and Graph-M). Across all models, relying solely on SMILES-based or graph-based metabolite features in combination with gene features consistently resulted in reduced performance. For example, in *e_coli_core*, the overall accuracy dropped from 77.35% (full model) to 70.34% (Ge-SMILES) and 74.33% (Ge-Graph). These results highlight that integrating both sequential and graph-based metabolite representations is critical for optimal performance.

Graph Representation Evaluation: We further examined the impact of different graph representations generated at early stages of the pipeline (\mathcal{G}_0 and \mathcal{G}_1). Across all metabolic models, using the early-stage representations resulted in decreased performance compared to the proposed graph representation. For instance, in *iMM904*, the overall accuracy was 82.02% for \mathcal{G}_0 , 84.70% for \mathcal{G}_1 , and 85.54% for the proposed representation. This demonstrates the importance of the proposed graph construction pipeline for capturing meaningful metabolic relationships.

Overall, the experimental results confirm that *GraphGDel* effectively integrates sequential and graph-based represen-

tations, leveraging the constructed graph to enhance gene deletion strategy prediction. The improvements are consistent across models of different sizes, indicating the generalizability and robustness of the framework.

V. DISCUSSION AND CONCLUSION

In this study, we address the gene deletion strategy prediction problem by introducing a graph-based representation approach. Specifically, we (1) propose a systematic pipeline for constructing graph representations from genome-scale metabolic models, and (2) develop *GraphGDel*, a learning framework that integrates sequential representations with graph-structural information to enhance gene deletion strategy prediction in genome-scale metabolic models.

In the computational experiments, we compared *GraphGDel* with two baseline methods (DNN and DeepGdel) on three constraint-based metabolic models of different scales. The results demonstrate the effectiveness of *GraphGDel* for predicting gene deletion strategies across models of varying sizes, consistently outperforming both baselines across all five evaluation metrics. Specifically, the overall accuracy of *GraphGDel* for *e_coli_core*, *iMM904*, and *iML1515* was 77.35%, 85.54%, and 73.22%, respectively, representing improvements over the DNN baseline (14.04%, 16.26%, and 13.18% higher) and the DeepGdel baseline (6.17%, 4.96%, and 5.31% higher).

We also conducted ablation studies to assess the impact of different learning modules on gene deletion strategy prediction performance. Using only SMILES-based metabolite features (Ge-SMILES) or graph-based metabolite features (Ge-Graph) resulted in consistent performance degradation across all metabolic models. These results highlight that integrating both sequential and graph-based metabolite representations is crucial for achieving optimal performance in gene deletion strategy prediction. Furthermore, our graph representation evaluation experiments highlight the importance of the proposed graph representations in graph-based learning tasks for metabolic models. The proposed framework, when learning from these graph representations, consistently achieves the best performance, whereas using representations from the early stages of the construction pipeline (\mathcal{G}_0 and \mathcal{G}_1) results in performance degradation. These findings demonstrate the value of a carefully designed graph representation construction pipeline.

The proposed graph representation construction pipeline generates graphs from genome-scale metabolic models by leveraging both graph-structural properties and metabolite knowledge to filter biochemical interactions, thereby enabling downstream graph-based learning tasks. Since genome-scale metabolic models encode more complex relationships among elements, such as GPR rules linking genes to reactions, the successful application of the proposed metabolite graph suggests the potential to integrate multiple types of relationships to further enhance gene deletion strategy prediction. For instance, the pipeline could be extended to construct multi-layered graphs where different node types represent metabolites, genes, and reactions, with edges capturing various relationships, including biochemical transformations and GPR rules.

A key innovation of *GraphGDel* is the explicit incorporation of graph structure information through the Graph-M module, addressing a limitation of previous approaches that relied solely on sequential data. By leveraging metabolic network

TABLE VII: Comparison of gene deletion strategy prediction performance between the proposed GraphGDel framework and two baseline methods across three metabolic models. “M-Avg.” denotes macro-averaged results. Best-performing values are shown in bold.

Metric	e_coli_core			iMM904			iML1515		
	DNN	DeepGdel	Proposed	DNN	DeepGdel	Proposed	DNN	DeepGdel	Proposed
Overall Accuracy (%)	63.31 \pm 2.70	71.18 \pm 0.44	77.35 \pm 1.45	69.28 \pm 1.58	80.58 \pm 0.44	85.54 \pm 1.04	60.04 \pm 1.04	67.91 \pm 0.34	73.22 \pm 1.02
M-Avg. Precision (%)	64.99 \pm 2.57	72.44 \pm 0.56	75.99 \pm 1.33	72.07 \pm 1.44	77.51 \pm 0.42	83.19 \pm 1.07	64.60 \pm 1.13	68.90 \pm 0.35	74.67 \pm 1.09
M-Avg. Recall (%)	64.13 \pm 2.20	72.87 \pm 0.54	75.38 \pm 1.37	68.52 \pm 1.36	77.85 \pm 0.44	82.91 \pm 1.12	61.80 \pm 1.11	64.40 \pm 0.35	72.51 \pm 1.06
M-Avg. F1 Score (%)	59.59 \pm 2.36	70.85 \pm 0.65	74.45 \pm 1.24	64.84 \pm 1.56	76.48 \pm 0.45	81.87 \pm 1.25	58.69 \pm 1.17	63.22 \pm 0.34	72.31 \pm 1.03
M-Avg. AUC (%)	62.66 \pm 2.89	71.16 \pm 0.85	76.56 \pm 1.26	66.50 \pm 1.47	80.24 \pm 0.78	84.24 \pm 1.12	60.30 \pm 1.14	65.78 \pm 0.54	73.17 \pm 1.04

TABLE VIII: Ablation study of the proposed framework comparing two variants: Ge-SMILES (using only gene and SMILES-based metabolite features) and Ge-Graph (using only gene and graph-based metabolite features). Results are evaluated across the three metabolic models under study. “M-Avg.” denotes macro-averaged results. Best-performing values are shown in bold.

Metric	e_coli_core			iMM904			iML1515		
	Ge-SMILES	Ge-Graph	Proposed	Ge-SMILES	Ge-Graph	Proposed	Ge-SMILES	Ge-Graph	Proposed
Overall Accuracy (%)	70.34 \pm 1.25	74.33 \pm 1.35	77.35 \pm 1.45	78.76 \pm 1.17	83.33 \pm 1.38	85.54 \pm 1.04	67.11 \pm 0.96	70.35 \pm 1.38	73.22 \pm 1.02
M-Avg. Precision (%)	70.34 \pm 1.26	72.72 \pm 1.55	75.99 \pm 1.33	78.34 \pm 1.12	81.74 \pm 1.37	83.19 \pm 1.07	68.45 \pm 0.94	71.49 \pm 1.36	74.67 \pm 1.09
M-Avg. Recall (%)	71.95 \pm 1.24	72.31 \pm 1.36	75.38 \pm 1.37	77.29 \pm 1.12	81.36 \pm 1.49	82.91 \pm 1.12	63.23 \pm 0.88	69.30 \pm 1.35	72.19 \pm 0.91
M-Avg. F1 Score (%)	70.23 \pm 1.22	71.24 \pm 1.54	74.45 \pm 1.24	77.44 \pm 1.15	80.93 \pm 1.22	81.87 \pm 1.25	62.13 \pm 0.93	69.45 \pm 1.45	72.31 \pm 1.03
M-Avg. AUC (%)	70.37 \pm 1.32	73.47 \pm 1.37	76.56 \pm 1.26	78.49 \pm 1.15	82.42 \pm 1.41	84.24 \pm 1.12	68.35 \pm 0.93	70.44 \pm 1.39	73.17 \pm 1.04

TABLE IX: Performance comparison of the proposed framework using different graph representations (\mathcal{G}_0 and \mathcal{G}_1) across three metabolic models. “M-Avg.” denotes macro-averaged results. The best-performing values are shown in bold.

Metric	e_coli_core			iMM904			iML1515		
	\mathcal{G}_0	\mathcal{G}_1	Proposed	\mathcal{G}_0	\mathcal{G}_1	Proposed	\mathcal{G}_0	\mathcal{G}_1	Proposed
Overall Accuracy (%)	73.25 \pm 1.45	76.20 \pm 1.50	77.35 \pm 1.45	82.02 \pm 1.04	84.70 \pm 1.05	85.54 \pm 1.04	70.15 \pm 1.02	72.80 \pm 1.00	73.22 \pm 1.02
M-Avg. Precision (%)	73.10 \pm 1.33	75.85 \pm 1.30	75.99 \pm 1.33	80.33 \pm 1.07	83.05 \pm 1.05	83.19 \pm 1.07	70.88 \pm 1.09	73.92 \pm 1.10	74.67 \pm 1.09
M-Avg. Recall (%)	73.55 \pm 1.37	75.45 \pm 1.38	75.38 \pm 1.37	81.01 \pm 1.12	83.10 \pm 1.10	82.91 \pm 1.12	68.42 \pm 0.91	72.51 \pm 0.93	72.19 \pm 0.91
M-Avg. F1 Score (%)	72.67 \pm 1.24	74.40 \pm 1.20	74.45 \pm 1.24	80.57 \pm 1.25	81.75 \pm 1.20	81.87 \pm 1.25	68.09 \pm 1.03	72.20 \pm 1.05	72.31 \pm 1.03
M-Avg. AUC (%)	73.12 \pm 1.26	76.10 \pm 1.20	76.56 \pm 1.26	81.55 \pm 1.12	83.70 \pm 1.10	84.24 \pm 1.12	69.67 \pm 1.04	72.85 \pm 1.02	73.17 \pm 1.04

topology, *GraphGDel* captures relationships between metabolites that are not apparent from their sequential representations. While this work uses LSTM autoencoders and Graph Convolutional Networks as the default architecture to demonstrate and benchmark the framework’s feasibility, its modular design allows for the integration of more advanced models. For example, one potential improvement is to incorporate recent large language models specialized for molecular or protein sequences into the learning modules of *GraphGDel*.

In future work, we will explore enhancing the graph representation construction pipeline to incorporate additional types of model elements, such as reactions and genes. Additionally, we will benchmark advanced deep learning architectures for metabolite and gene representation learning within the proposed framework across metabolic models from a broader range of species.

VI. ACKNOWLEDGMENTS

This work was supported in part by JSPS, KAKENHI under Grant 23K20386, and JST SPRING, Grant Number JP-MJSP2110.

REFERENCES

- Otero-Muras, I. & Carbonell, P. Automated engineering of synthetic metabolic pathways for efficient biomanufacturing. *Metabolic Engineering* **63**, 61–80 (2021).
- García-Jiménez, B., Torres-Bacete, J. & Nogales, J. Metabolic modelling approaches for describing and engineering microbial communities. *Computational and Structural Biotechnology Journal* **19**, 226–246 (2021).
- Foster, C. J., Wang, L., Dinh, H. V., Suthers, P. F. & Maranas, C. D. Building kinetic models for metabolic engineering. *Current Opinion in Biotechnology* **67**, 35–41 (2021).
- Toya, Y. & Shimizu, H. Flux analysis and metabolomics for systematic metabolic engineering of microorganisms. *Biotechnology advances* **31**, 818–826 (2013).
- Pharkya, P. & Maranas, C. D. An optimization framework for identifying reaction activation/inhibition or elimination candidates for overproduction in microbial systems. *Metabolic engineering* **8**, 1–13 (2006).
- Vieira, V., Maia, P., Rocha, M. & Rocha, I. Comparison of pathway analysis and constraint-based methods for cell factory design. *BMC bioinformatics* **20**, 1–15 (2019).
- Ranganathan, S., Suthers, P. F. & Maranas, C. D. Optforce: an optimization procedure for identifying all genetic manipulations leading to targeted overproductions. *PLoS computational biology* **6**, e1000744 (2010).
- Lewis, N. E. *et al.* Omic data from evolved *e. coli* are consistent with computed optimal growth from genome-scale models. *Molecular systems biology* **6**, 390 (2010).
- Yang, L., Cluett, W. R. & Mahadevan, R. Emilio: a fast algorithm for genome-scale strain design. *Metabolic engineering* **13**, 272–281 (2011).
- Egen, D. & Lun, D. S. Truncated branch and bound achieves efficient constraint-based genetic design. *Bioinformatics* **28**, 1619–1623 (2012).
- Rockwell, G., Guido, N. J. & Church, G. M. Redirector: designing cell factories by reconstructing the metabolic objective. *PLoS computational biology* **9**, e1002882 (2013).
- Ohno, S., Shimizu, H. & Furusawa, C. Fastpros: screening of reaction knockout strategies for metabolic engineering. *Bioinformatics* **30**, 981–987 (2014).
- Gu, D., Zhang, C., Zhou, S., Wei, L. & Hua, Q. Idealknock: a framework for efficiently identifying knockout strategies leading to targeted overproduction. *Computational biology and chemistry* **61**, 229–237 (2016).
- Tamura, T. Grid-based computational methods for the design of constraint-based parsimonious chemical reaction networks to simulate metabolite production: Gridprod. *BMC bioinformatics* **19**, 1–9 (2018).

[15] Tamura, T., Muto-Fujita, A., Tohsato, Y. & Kosaka, T. Gene deletion algorithms for minimum reaction network design by mixed-integer linear programming for metabolite production in constraint-based models: gdel_minrn. *Journal of Computational Biology* **30**, 553–568 (2023).

[16] Trinh, C. T., Unrean, P. & Srienc, F. Minimal escherichia coli cell for the most efficient production of ethanol from hexoses and pentoses. *Applied and environmental microbiology* **74**, 3634–3643 (2008).

[17] Schneider, P., von Kamp, A. & Klamt, S. An extended and generalized framework for the calculation of metabolic intervention strategies based on minimal cut sets. *PLoS computational biology* **16**, e1008110 (2020).

[18] Banerjee, D. *et al.* Genome-scale metabolic rewiring improves titers rates and yields of the non-native product indigoidine at scale. *Nature communications* **11**, 5385 (2020).

[19] Tamura, T. Metnetcomp: Database for minimal and maximal gene-deletion strategies for growth-coupled production of genome-scale metabolic networks. *IEEE/ACM Transactions on Computational Biology and Bioinformatics* (2023).

[20] Yang, Z. & Tamura, T. Dbgdel: Database-enhanced gene deletion framework for growth-coupled production in genome-scale metabolic models. *IEEE Transactions on Computational Biology and Bioinformatics* (2025).

[21] Yang, Z. & Tamura, T. Deepgdel: Deep learning-based gene deletion prediction framework for growth-coupled production in genome-scale metabolic models. *arXiv preprint arXiv:2504.06316* (2025).

[22] LeCun, Y., Bengio, Y. & Hinton, G. Deep learning. *nature* **521**, 436–444 (2015).

[23] Stelling, J., Klamt, S., Bettenbrock, K., Schuster, S. & Gilles, E. D. Metabolic network structure determines key aspects of functionality and regulation. *Nature* **420**, 190–193 (2002).

[24] Wang, Y.-P. & Lei, Q.-Y. Metabolite sensing and signaling in cell metabolism. *Signal transduction and targeted therapy* **3**, 30 (2018).

[25] Jeong, H., Tombor, B., Albert, R., Oltvai, Z. N. & Barabási, A.-L. The large-scale organization of metabolic networks. *Nature* **407**, 651–654 (2000).

[26] Li, R. *et al.* Graph signal processing, graph neural network and graph learning on biological data: a systematic review. *IEEE Reviews in Biomedical Engineering* **16**, 109–135 (2021).

[27] Muzio, G., O’Bray, L. & Borgwardt, K. Biological network analysis with deep learning. *Briefings in bioinformatics* **22**, 1515–1530 (2021).

[28] Jin, S., Zeng, X., Xia, F., Huang, W. & Liu, X. Application of deep learning methods in biological networks. *Briefings in bioinformatics* **22**, 1902–1917 (2021).

[29] Kanehisa, M. & Goto, S. Kegg: kyoto encyclopedia of genes and genomes. *Nucleic acids research* **28**, 27–30 (2000).

[30] Orth, J. D., Thiele, I. & Palsson, B. Ø. What is flux balance analysis? *Nature biotechnology* **28**, 245–248 (2010).

[31] Simeonidis, E. & Price, N. D. Genome-scale modeling for metabolic engineering. *Journal of Industrial Microbiology and Biotechnology* **42**, 327–338 (2015).

[32] Pfeiffer, T., Soyer, O. S. & Bonhoeffer, S. The evolution of connectivity in metabolic networks. *PLoS biology* **3**, e228 (2005).

[33] King, Z. A. *et al.* Bigg models: A platform for integrating, standardizing and sharing genome-scale models. *Nucleic acids research* **44**, D515–D522 (2016).

[34] Schneider, P., Mahadevan, R. & Klamt, S. Systematizing the different notions of growth-coupled product synthesis and a single framework for computing corresponding strain designs. *Biotechnology Journal* **16**, 2100236 (2021).

[35] Alter, T. B. & Ebert, B. E. Determination of growth-coupling strategies and their underlying principles. *BMC bioinformatics* **20**, 1–17 (2019).

[36] Weininger, D. Smiles, a chemical language and information system. 1. introduction to methodology and encoding rules. *Journal of chemical information and computer sciences* **28**, 31–36 (1988).

[37] Hochreiter, S. & Schmidhuber, J. Long short-term memory. *Neural Computation* **9**, 1735–1780 (1997).

[38] Sutskever, I., Vinyals, O. & Le, Q. V. Sequence to sequence learning with neural networks. *Advances in neural information processing systems* **27** (2014).

[39] Vaswani, A. *et al.* Attention is all you need. *Advances in neural information processing systems* **30** (2017).

[40] Orth, J. D., Fleming, R. M. & Palsson, B. Ø. Reconstruction and use of microbial metabolic networks: the core escherichia coli metabolic model as an educational guide. *EcoSal plus* **4**, 10–1128 (2010).

[41] Mo, M. L., Palsson, B. Ø. & Herrgård, M. J. Connecting extracellular metabolomic measurements to intracellular flux states in yeast. *BMC systems biology* **3**, 1–17 (2009).

[42] Monk, J. M. *et al.* iml1515, a knowledgebase that computes escherichia coli traits. *Nature biotechnology* **35**, 904–908 (2017).

[43] Wang, S., Guo, Y., Wang, Y., Sun, H. & Huang, J. Smiles-bert: large scale unsupervised pre-training for molecular property prediction. In *Proceedings of the 10th ACM international conference on bioinformatics, computational biology and health informatics*, 429–436 (2019).

[44] Hirohara, M., Saito, Y., Koda, Y., Sato, K. & Sakakibara, Y. Convolutional neural network based on smiles representation of compounds for detecting chemical motif. *BMC bioinformatics* **19**, 526 (2018).

[45] Pinheiro, G. A. *et al.* Machine learning prediction of nine molecular properties based on the smiles representation of the qm9 quantum-chemistry dataset. *The Journal of Physical Chemistry A* **124**, 9854–9866 (2020).

[46] Moretti, S., Tran, V. D. T., Mehl, F., Ibberson, M. & Pagni, M. Metanetx/mnxref: unified namespace for metabolites and biochemical reactions in the context of metabolic models. *Nucleic acids research* **49**, D570–D574 (2021).

[47] Tran, N. H., Zhang, X., Xin, L., Shan, B. & Li, M. De novo peptide sequencing by deep learning. *Proceedings of the National Academy of Sciences* **114**, 8247–8252 (2017).

[48] You, Z.-H., Lei, Y.-K., Zhu, L., Xia, J. & Wang, B. Prediction of protein-protein interactions from amino acid sequences with ensemble extreme learning machines and principal component analysis. *BMC bioinformatics* **14**, S10 (2013).

[49] ELAbd, H. *et al.* Amino acid encoding for deep learning applications. *BMC bioinformatics* **21**, 235 (2020).

[50] Paszke, A. Pytorch: An imperative style, high-performance deep learning library. *arXiv preprint arXiv:1912.01703* (2019).